Computers and Electrical Engineering 40 (2014) 215–226

Contents lists available at ScienceDirect

Computers and Electrical Engineering

journal homepage: www.elsevier.com/locate/compeleceng

A dynamic non-circular iris localization technique for non-ideal data ☆

Farmanullah Jan [a,c,*], Imran Usman [b], Shahid A. Khan [a], Shahzad A. Malik [a]

[a] Department of Electrical Engineering, COMSATS Institute of Information Technology, Park Road, Chak Shahzad, 44000 Islamabad, Pakistan
[b] Center for Advanced Studies in Telecommunications, COMSATS Institute of Information Technology, Park Road, Chak Shahzad, 44000 Islamabad, Pakistan
[c] Department of Physics, COMSATS Institute of Information Technology, Park Road, Chak Shahzad, 44000 Islamabad, Pakistan

ARTICLE INFO

Article history:
Received 13 July 2012
Received in revised form 12 May 2014
Accepted 12 May 2014
Available online 2 June 2014

ABSTRACT

Iris localization plays a decisive role in the overall iris biometric system's performance, because it isolates the valid part of iris. This study proposes a reliable iris localization technique. It includes the following. First, it extracts the iris inner contour within a sliding-window in an eye image using a multi-valued adaptive threshold and the two-dimensional (2D) properties of binary objects. Then, it localizes the iris outer contour using an edge-detecting operator in a sub image centered at the pupil center. Finally, it regularizes the iris contours to compensate for their non-circular structure. The proposed technique is tested on the following public iris databases: CASA V1.0, CASIA-Iris-Lamp, IITD V1.0, and the MMU V1.0. The experimental and accuracy results of the proposed scheme compared with other state-of-the-art techniques endorse its satisfactory performance.

1. Introduction

Reliable recognition of individuals has long been an aspiration of the government and public sectors, where most often humans are recognized using the conventional security measures [1–5]. Literature reveals that these conventional type systems are not foolproof because they rely on the knowledge (e.g., passwords) and/or tokens (e.g., passports) based techniques, which could be lost, hacked, shared, or duplicated artificially [5]. Therefore, for authentic recognition, the research community diverted towards the biometric technology, which is currently functional in numerous countries: Australia, Canada, Gambia, and among others. It applies mathematical operations on the physical and/or physiological traits (e.g., retina, iris, gait, ear, fingerprint, etc.) of humans for identification [6]. The fingerprint, voice, signature, and face have long been in use for the human identification [7], but they change with the aging affects [5]. On the other hand, the iris remains almost stable and unique over the entire life of a subject, except some minor changes occurring in early life [8]. Iris is an annulus between the pupil and sclera, which is protected by the cornea. It has relatively a complex structure that includes the corona, freckles, ridges, furrows, crypts, and arching ligaments [5,8]. Due to its structure complexity, the iris pattern could not be duplicated artificially, except a subject's intentional surgery [5,8]. Iris biometric has numerous applications, e.g., the auto teller machines, accessing a restricted zone, and border-crossing control are to name a few.

Commercial iris biometric systems are typically based on Daugman [9] and/or Wildes' [8] algorithms, which are reported in literature with great accuracy [5]. However, they work under very constrained environment. For example, a subject

☆ Reviews processed and approved for publication by Editor-in-Chief Dr. Manu Malek.

* Corresponding author at: Department of Physics, COMSATS Institute of Information Technology, Park Road, Chak Shahzad, 44000 Islamabad, Pakistan. Tel.: +92 47000 3x244.
E-mail addresses: farmanullah_jan@comsats.edu.pk, farmanullahs123@gmail.com (F. Jan).

http://dx.doi.org/10.1016/j.compeleceng.2014.05.004
0045-7906/

wearing no eyeglasses or contact lenses stands at a short distance and glares directly into the camera, with no gaze-view. However, their performance strongly deteriorates while dealing with the non-ideal data containing noisy issues, such as rotated-irises (i.e., eye not oriented horizontally in an eye image), specular reflections, blurring, non-uniform illumination; hair, glasses, contact lenses, eyelids, and eyelashes [6]. The main reason behind a system's poor performance is tied with its iris segmentation algorithm that is generally developed under ideal environment [5]. Iris segmentation localizes the iris inner and outer contours at the pupil and sclera, respectively, and detects and excludes any other superimposing noise, e.g., eyelids [5]. Notably, the iris localization task plays an indispensable role because it demarcates boundaries of the valid iris part. Therefore, this study focuses on localizing the iris contours only, however to remove the other unwanted iris parts (e.g., eyelids), please refer to the published work [5].

State-of-the-art iris localization techniques include the gradients and edge-detectors [5,6], active contour models [5,6], histogram and thresholding [5,6], and among others. Daugman [9] used a circular Integro-differential operator (IDO) to localize iris with a circle approximation. Similarly, Wildes [8] adopted a combination of the edge-map and the circular Hough transform (CHT) to localize iris. An implicit flaw in these methods [8,9], is their poor performance for the rotated-irises, because they are specifically biased for the horizontal direction only. It is because that in the vertical direction, the iris contours are usually occluded by eyelids. Moreover, this kind of issue also exists in numerous articles [7,10,11]. Khan et al. [7] localize iris using a combination of the histogram-bisection and the gradients based technique. However, to localize the iris inner contour, they first convert the input eye image to a binary image and then localize the accurate pupil object based on the *eccentricity*. This idea does not work well for a binary image where the pupil object is surrounded by other low intensity regions (e.g., eyebrows). It is because that eccentricity of a small round object may be smaller than that of the actual pupil object, which may not be quite round due to the non-uniform illumination. Similarly, Ibrahim et al. [10] use the *standard-deviation* of the *xy*-coordinates of pixels in a binary object to localize pupil in binary image. However, its performance also degrades for a binary image suffered by the mentioned issue. Therefore, to resolve these highlighted issues, this study proposes a reliable iris localization technique. It includes the following. First, it localizes the iris inner contour within a sliding-window using a multi-valued adaptive threshold and 2D object properties. Then, it extracts a sub image centered at the pupil center. After that, it localizes the iris outer contour within a sub image using IDO. Finally, it regularizes the iris contours to compensate for their non-circular nature.

The remainder of this paper is organized as follows. Section 2 explains different modules of the proposed technique explicitly. Section 3 thoroughly explains its experimental results. Finally, Section 4 concludes the proposed work.

2. Design and structure of the proposed technique

The proposed iris localization technique comprises the following modules: iris inner contour, iris outer contour, and contours regularization. Its procedure (Fig. 1) is explicitly detailed in the following text.

2.1. Iris inner contour

As shown in Fig. 2(a), an eye image generally contains the dark and bright regions. The pupil, eyelashes, eyelids, eyebrows, and hair, are relatively dark regions compared with the sclera, specular reflections, and probably the skin. Therefore, the presence of any of these dark regions in an eye image generally complicates pupil localization. Fortunately, the pupil region is relatively compact compared with other low intensity regions. To resolve this issue, this paper offers a reliable technique to localize iris inner contour with a circle approximation (x_p, y_p, r_p). Where (x_p, y_p) and (r_p) represent the center and radius parameters of the pupil circle, respectively. It includes the following steps:

1. Create a sliding-window $S_w(x, y)$ having each side length equal to $0.5W$, where W is the width of an input eye image $I(x, y)$. Mark three horizontal rows at different discrete positions in $I(x, y)$ (see Fig. 2(b)) and initialize the iteration-index $(\tilde{q})$ to one as well.
2. Place $S_w(x, y)$ at a discrete location $(x_s(i_1), y_s(i_2))$ in $I(x, y)$, where the indexing parameters i_1 and i_2 are both initially set to one and:

$$x_s = \{0.25W, 0.25W + 30, 0.25W + 60, \ldots, s_o\}, \tag{1}$$

$$y_s = \{0.25W, 0.50W, 0.75W\}, \tag{2}$$

where $s_o = L - 0.25W$, L as length of $I(x, y)$. Fig. 2(b) shows a sample image depicting $S_w(x, y)$ located at some discrete locations along the first, second, and third rows.

3. Convert $S_w(x, y)$ (see Fig. 4) to a binary image $bw(x, y)$ via the following multi-valued adaptive threshold (λ) as

$$bw(x, y) = \begin{cases} 1 & \text{if } S_w(x, y) < \lambda_k \\ 0 & \text{otherwise} \end{cases}, \tag{3}$$

$$\lambda_k = \Omega + k, \quad \text{for} \quad k = 0, 1, 2, \ldots, 0.05\Omega, \tag{4}$$

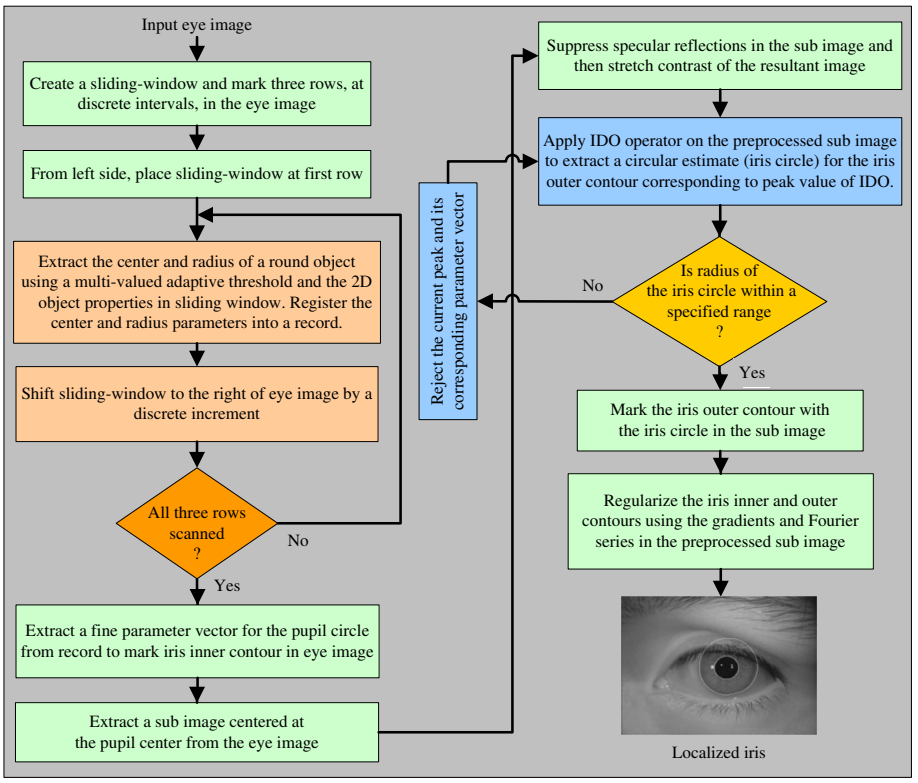

Fig. 1. Block diagram of the proposed iris localization technique.

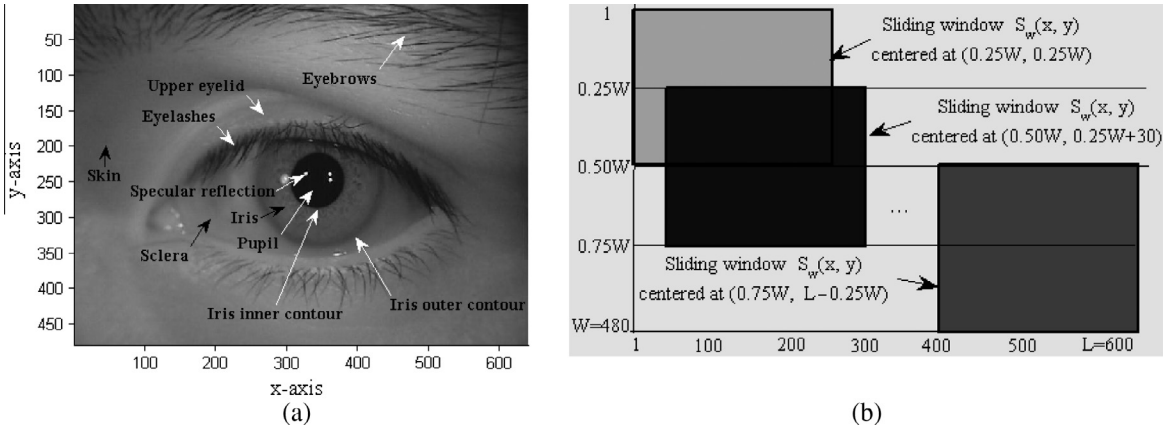

Fig. 2. (a) Different parts in an eye image. Eye image is taken from the CASIA-Iris-Lamp [12]. (b) Sample image showing shifts of the sliding window $S_w(x, y)$ at some discrete locations along three horizontal rows.

where Ω is the lower gray level saturated limit of $I(x, y)$ [6]. It represents the saturated gray level value of the bottom 1% of all the gray values in $I(x, y)$. Parameter k, initially set to zero, is used to compensate for any possible gray level variations in pupil. Fig. 3 shows the position of Ω in the histogram of $I(x, y)$.

4. Use a combination of the 4-connectivity procedure and a bilinear interpolation [13] to detect and fill the holes in $bw(x, y)$. Then, pass the resultant image through a morphological *open* [13] operator, with a structuring element having radius three, to isolate any loosely connected objects. In a binary image, a region of zeros (i.e., 0s) surrounded by ones (i.e., 1s) and not accessible from the image's dimensions is called a hole. Similarly, a region of ones is called an object [13]. Following that argument, detect all binary objects in $bw(x, y)$ and use the following sub steps, assuming $\widetilde{N}$ objects in $bw(x, y)$, to localize a round object, i.e., possibly the pupil object:

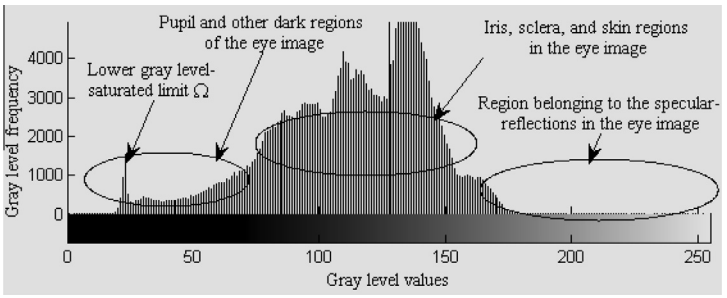

Fig. 3. Histogram of $I(x, y)$ showing locations of Ω; pupil and dark regions; iris, sclera, and skin regions; and specular reflections.

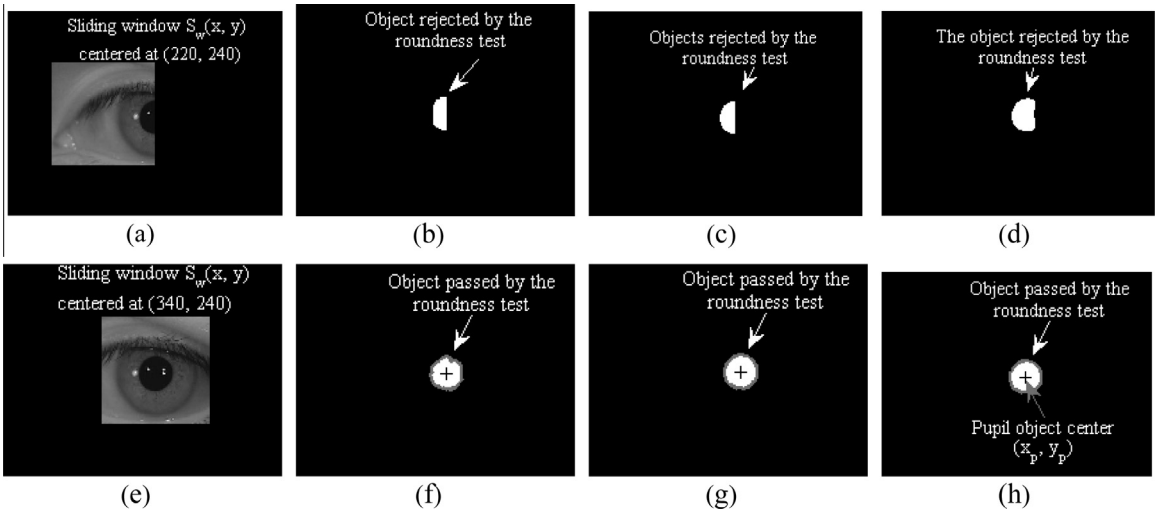

Fig. 4. (a) $S_w(x, y)$ centered at (220, 240) along the second line in $I(x, y)$. It contains partial pupil inside. (b–d) $bw(x, y)$ for some discrete values of k where a detected object is rejected by the roundness test. (e) $S_w(x, y)$ centered at (340, 240) along second line in $I(x, y)$, it contains complete pupil region inside. (f–h) $bw(x, y)$ wherein the detected object is passed by roundness test.

a. Compute the coarse length (b_1) and width (b_2) of a jth object (j is initially set to one) as

$$(b_1, b_2) = (\max(x_{\max} - x_{\min}, y_{\max} - y_{\min}),\ \min(x_{\max} - x_{\min}, y_{\max} - y_{\min})), \tag{5}$$

where

$$(x_{\min}, y_{\min}) = (\min(X), \min(Y)), \tag{6}$$

$$(x_{\max}, y_{\max}) = (\max(X), \max(Y)), \tag{7}$$

and the arrays X and Y hold the x- and y-coordinates of the boundary pixels of this object, respectively. Next, we define a *roundness-test* ($\hat{f}$) as

$$\hat{f} = (0.6b_1 \le b_2 \le b_1). \tag{8}$$

b. If $\hat{f}$ is one, then compute the center of mass (x_o, y_o) [13] for this object using Eq. (9). Generally, the physical concept of the center of mass refers to a point on an object having the same portion of object around it in any direction. It is defined as

$$(x_o, y_o) = \left(\frac{1}{K_o}\sum_{i=1}^{K_o} x_i,\ \frac{1}{K_o}\sum_{i=1}^{K_o} y_i\right), \tag{9}$$

where K_o is the number of pixels located at discrete points, $(x_1, y_1), (x_2, y_2), \ldots, (x_{K_o}, y_{k_o})$, in the current object. Similarly, compute its coarse radius (r_o) as

$$r_o = 0.5(0.5(x_{\max} - x_{\min}) + 0.5(y_{\max} - y_{\min})). \tag{10}$$

Then, register the center of mass and radius as $(X(j), Y(j), R(j)) = (x_o, y_o, r_o)$. Repeat this process from the Step-a for the other values of j as well.

Finally, extract the best possible circular parameter vector as
if (R is not empty) **then**

$$\overline{R}(\tilde{q}) = \max_{\forall j \in \{1,2,\ldots,\widetilde{N}\}} \{R\}, \tag{11}$$

$$(\overline{X}(\tilde{q}), \overline{Y}(\tilde{q})) = (X(j_o), Y(j_o)), \tag{12}$$

where $j_o \in \{1, 2, 3, \ldots, \widetilde{N}\}$ such that $R(j)$ is maximum at $j = j_o$. The arrays $\overline{R}$, $\overline{X}$, and $\overline{Y}$ hold the coarse radius and center parameters, respectively, for a fair round object for the $\tilde{q}$th iteration.
end

5. Increment $\tilde{q}$ by one and repeat this process from Step-3 for the other values of k as well. After that, shift the sliding window to a next location thereby adjusting the values of i_1 and i_2, and then repeat the entire process from Step-2. This process is continued until the entire image is scanned. Finally, extract a fine parameter (x_p, y_p, r_p) as

if ($\overline{R}$ is not empty) **then**

$$r_p = \max_{\forall \tilde{q}} \{\overline{R}\}, \tag{13}$$

$$(x_p, y_p) = (\overline{X}(s), \overline{Y}(s)), \tag{14}$$

where s is the location at which $\overline{R}$ is maximum.
end

Fig. 4(a) shows $S_w(x, y)$ centered at (220,240) along the second line, where it contains the partial pupil inside. Fig. 4(b)–(d) shows the detected object in $bw(x, y)$ for some discrete values of k. In each case, detected object is rejected by the test embedded in Eq. (8). It is because that its length to width ratio does not fulfill the preset criterion. Similarly, Fig. 4(e) shows $S_w(x,y)$ centered at (340,240) along the second line in $I(x, y)$, which now contains the entire pupil region inside. Fig. 4(f)–(h) shows $bw(x,y)$ containing the detected object, which is passed by the stated test. Finally, Fig. 5 shows the iris inner contour accurately marked with (x_p,y_p,r_p).

2.2. Iris outer contour

After marking iris inner contour with (x_p, y_p, r_p), the next turn is to mark the iris outer contour. In non-ideal data, eyelashes, glasses, hair, and the eyelids usually obscure the iris region [3,6]. Besides, the low contrast between the sclera and iris compared with the pupil and iris, and the rotated-iris eye images may also hurdle in the iris localization. To resolve this issue, this study proposes a reliable technique. It includes extracting a sub image centered at pupil center, suppressing specular reflections, and adopting the IDO to localize the iris outer contour with (x_i, y_i, r_i). Where (x_i, y_i) and (r_i) represent the center and radius of iris circle, respectively.

Integro-differential operator (*IDO*): it has been used by numerous researchers [6,10,22–24] to localize circular iris contours, which is defined as

$$\max_{(x_i,y_i,r_i)} \left| G_\sigma(r) * \frac{\delta}{\delta r} \oint_{(x_i,y_i,r_i)} \frac{w(x,y)}{2\pi r} ds \right|, \tag{15}$$

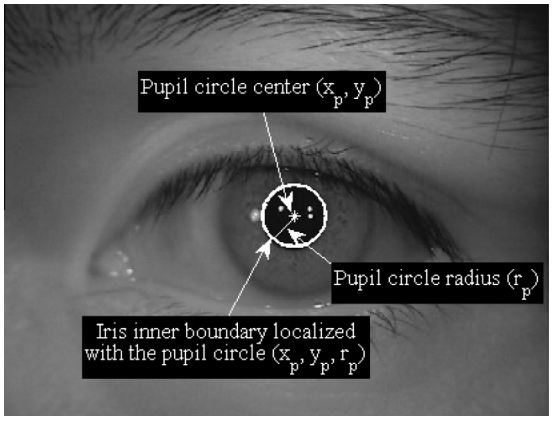

Fig. 5. Inner contour marked with (x_p, y_p, r_p).

where $*$ represents the convolution operation [13], $w(x, y)$ the gray level value, $G_\sigma(r)$ the Gaussian smoothening filter with standard deviation 2 and window size (3×3), and (x_i, y_i) and r_i are the center and radius, respectively, of the iris circle. In the image $w(x, y)$, IDO searches for a target circle by increasing its radius from a lower limit (a_1) to an upper limit (a_2). As the literature [7,10] shows that the ratio between the pupil and iris circles is normally 1:3, therefore, set the radii range for the iris circle as $(a_1 \sim a_2) = (1.1r_p \sim 3.5r_p)$. Notably, such a range is indispensable while localizing the iris circle using IDO [5,6]. As the centers of the pupil and iris circles are close to each other, therefore, for fast processing, limit searching window of iris circle (x_i, y_i, r_i) as

$$((x_p - 6 < x_i < x_p + 6)\&(y_p - 6 < y_i < y_p + 6)).$$

Now to extract (x_i, y_i, r_i) for the iris circle, proceed with the following steps:

1. Extract a sub image $s(x, y)$ (see Fig. 6(a)) centered at (x_p, y_p) and having each side equal to $8r_p$ from $I(x, y)$. As mentioned earlier, argument behind this setting is the fact that the ratio between the pupil and iris circles radii is 1:3. However, to be on safe side, the length of each side of $I(x, y)$ is set to be 8 times of r_p.
2. As stated earlier, IDO is sensitive to specular reflections. Therefore, prior to localize the iris circle, suppress reflections. First, complement $s(x, y)$. Next, use a morphological '*imfill*' [6] operator to fill holes in resultant image $s_o(x, y)$ (see Fig. 6(b)). Then, pass $s_o(x, y)$ through a median filter having window size (15×15) to calm down any rapid gray level variations. The resultant image is $\hat{s}_o(x, y)$ (see Fig. 6(c)). Finally, stretch contrast of $\hat{s}_o(x, y)$ as

$$s_m(x, y) = 255\left\lceil \frac{\hat{s}_o(x, y) - d_1}{d_2 - d_1} \right\rceil, \tag{16}$$

   where d_1 and d_2 represent the minimum and maximum gray level values in $\hat{s}_o(x, y)$, respectively. The resultant preprocessed sub image is $s_m(x, y)$, see Fig. 6(d).
3. To speed localization process, scale down $s_m(x, y)$ by a scaling factor $(\varsigma = 0.5)$ [5]. The resultant image is $s_{sld}(x, y)$. Then, adopt the following sub steps to extract (x_i, y_i, r_i):
   a. Obtain a location (x_i, y_i, r_i) corresponding to the maximum value (Ψ) of IDO in $s_{sld}(x, y)$.
   b. Next, pass (x_i, y_i, r_i) through the following *Radial-test* as

$$\chi_1 = (1.1r_p < r_i \leq 3.5r_p). \tag{17}$$

The criterion embedded in χ_1 ensures that the iris circle must be bigger than the pupil circle, but smaller than its 3.5 times. Therefore, if χ_1 is one, then (x_i, y_i, r_i) represents the accurate iris circle. Otherwise, reject Ψ and repeat this process from Step-a. This process is continued until a fine (x_i, y_i, r_i) is localized or no circle is localized at all for the subsequent 20–50 peaks of IDO. If nor circle is localized, then the system aborts this process because of the image low quality, e.g., a closed eye or severely occluded iris [5,6]. Fig. 7(d) shows iris outer contour localized with (x_i, y_i, r_i).

2.3. Contours regularization

Literature [5,6] reveals that the iris inner and outer contours do not maintain any predetermined shape (e.g., circular/elliptical). Therefore, these contours need some sort of the flexible curves, e.g., snakes [5]. To resolve this issue, this study uses an effective technique comprising the gradients and Fourier series to regularize the iris contours in $s_m(x, y)$. To begin with, use the following steps:

1. As illustrated in Fig. 7(c), a gradient transition along the radial-segments around the iris inner boundary is generally strong. Based on this logic, extract a set of points having maximum radial gradients around the iris inner contour. First, imagine an annular strip centered at (x_p, y_p), which has pupil circle at its middle. Next, divide this strip into n_o radial segments oriented at discrete angles (θ_k), for $k = 0, 1, 2, \ldots, n_o - 1$, where n_o is set to the perimeter of the pupil circle, i.e., $n_o = 2\pi r_p$, and:

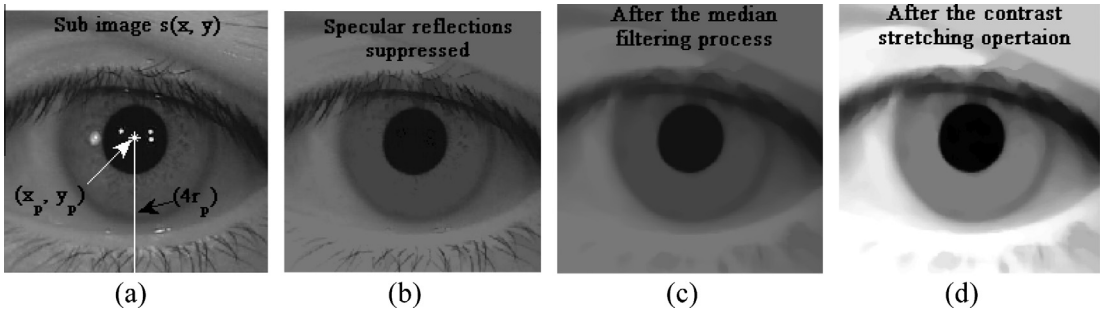

Fig. 6. (a) $s(x, y)$ extracted from $I(x, y)$. (b) $s_o(x, y)$ showing no specular reflections. (c) Median filtered image $\hat{s}_o(x, y)$. (d) $s_m(x, y)$ after the contrast stretching operation.

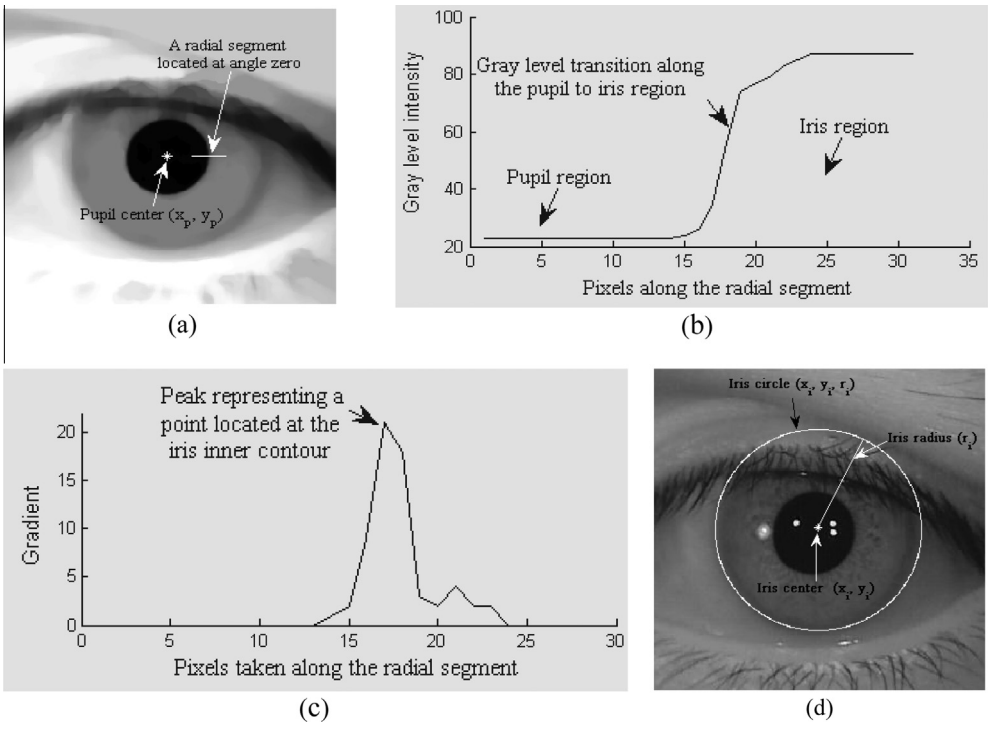

Fig. 7. (a) A radial segment oriented at angle zero with respect to (x_p, y_p), which is taken as a reference point in $s_m(x, y)$; the length of this segment is taken slightly larger than the proposed length for the sake of visual convenience only (b) 1D gray level profile of pixels along radial segment in (a). (c) Absolute 1D gradient profile of case in (b). (d) Iris outer contour localized with (x_i, y_i, r_i) in $s(x, y)$.

$$\theta_k = k\left(\frac{2\pi}{n_o}\right), \quad \text{for} \quad k = 0, 1, 2, \ldots, n_o - 1. \tag{18}$$

Then, extract the gray values of pixels located along all radial segments into an array (g) as

$$g(k, v) = s_m(x_v, y_v), \quad \text{for} \quad k = 0, 1, 2, \ldots, n_o - 1 \text{ and } v = 0, 1, 2, \ldots, m_o, \tag{19}$$

where m_o is length of radial-array $(\hat{r})$ and the parametric form of $x_v y_v$-coordinates are as $(x_v, y_v) = (x_p + \hat{r}_v \cos\theta_k, y_p + \hat{r}_v \sin\theta_k)$. Where $\hat{r} = \{r_p - 6, r_p - 5, \ldots, r_p, \ldots, r_p + 5, r_p + 6\}$ and r_p is radius of the pupil circle. Then, compute a gradient-array (Δ_g) as

$$\Delta_g(k, v) = g(k + 1, v + 1) - g(k, v), \quad \text{for} \quad k = 0, 1, 2, \ldots, n_o - 1 \quad \text{and} \quad v = 0, 1, 2, \ldots, m_o - 1. \tag{20}$$

Following that, compute the absolute blur $(\widehat{B})$ as

$$\widehat{B}(k, v) = G_\sigma * |\Delta_g(k, v)|, \quad \text{for} \quad k = 0, 1, 2, \ldots, n_o - 1 \quad \text{and} \quad v = 0, 1, 2, \ldots, m_o - 1, \tag{21}$$

where G_σ is a 1D Gaussian filtering process with standard deviation $\sigma = 2$ and window size (1×3), and * represents convolution between G_σ and $|\Delta_g(k, v)|$.

2. Extract radial distances of points having gradient-maxima around iris inner contour as
for $(k = 0$ to $n_o - 1)$

$$d_\theta(k) = \hat{r}(v_o), \tag{22}$$

where $v_o \in \{0, 1, 2, \ldots, m_o - 1\}$ such that $\widehat{B}(k, v)$ is maximum at $v = v_o$.
end

In Eq. (22), the array d_θ contains radial distances of n_o points located around iris inner contour, with reference to (x_p, y_p). As these distances may contain any sharp fluctuations, therefore, to get a smooth and close contour, filter d_θ through the Fourier series as follows:

First, extract a set of M discrete Fourier series coefficients (c_s) using the following expression. Where M controls a contour's fidelity, which is experimentally set to 25 [14].

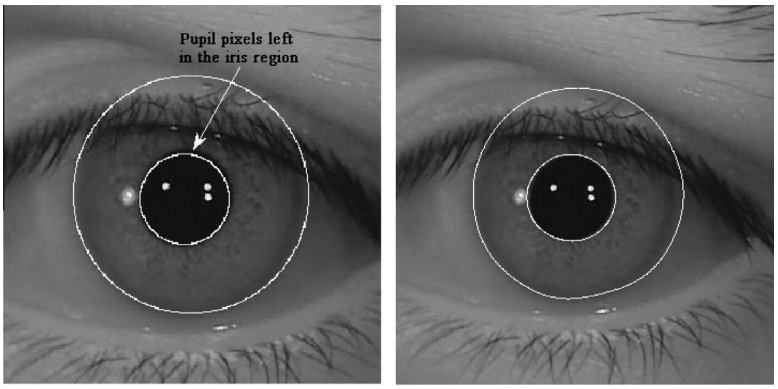

Fig. 8. (a) Iris localized with circle approximation in $s(x, y)$; some pupil pixels are left inside the iris. (b) Iris boundaries are regularized in $s(x, y)$.

$$c_s = \sum_{z=0}^{n_o-1} \widehat{B}_z \exp\left(-\frac{2\pi isz}{n_o}\right), \quad \text{for} \quad s = 0, 1, 2, \ldots, M-1. \tag{23}$$

Then, get a smooth and close contour (B) by putting c_s in the following expression as

$$B(t) = \frac{1}{n_o} \sum_{q=0}^{M-1} C_q \exp\left(\frac{2\pi iqt}{n_o}\right), \quad \text{for} \quad t = 0, 1, 2, \ldots, n_o - 1. \tag{24}$$

Finally, extract xy-coordinates of the iris inner contour as

$$(x_k, y_k) = (x_p + B_k \cos\theta_k, y_p + B_k \sin\theta_k), \quad \text{for} \quad k = 0, 1, 2, \ldots, n_o - 1. \tag{25}$$

Similarly, regularize the iris outer contour for $M = 30$. Fig. 8(a) shows the iris contours localized with circle approximation, where a significant portion of the pupil region is left unmarked in iris that affects the overall system's accuracy if not removed. Fig. 8(b) shows the iris inner and outer contours after regularization, which are now relatively better.

3. Experimental results and discussion

The proposed scheme is implemented in the MATLAB V 7.1, 2.33 GHz CPU with 2 GB RAM, and a set of the standard iris databases: CASA V1.0 [12], CASIA-Iris-Lamp [12], IITD V1.0 [6], and MMU V1.0 [6]. Images in these databases were acquired with the near infrared (NIR) illumination. NIR is preferred for the proposed technique because it reveals more iris texture compared with the visible wavelength (VW) illumination and is handy for the dark irises as well [9].

3.1. Experimental Setup-I

In this setup, we used the CASIA V1.0 iris database [12] that includes 756 eye images. In each image, the pupil region was manually edited to delete specular reflections and stored in the BMP format with resolution 320 × 280 pixel. Images, in this database, contain eyelashes, eyelids, and rotated-irises. For experimentations, all images were used and the *accuracy rate* (χ_r) [10] was used as a metric to measure accuracy of the proposed technique, which is defined as

$$\chi_r = \left(\frac{N_1}{N_T} \times 100\right), \tag{26}$$

where N_1 represents the number of correctly localized irises and N_T is the total number of images used in experimentation. χ_r depends on the *accuracy-error* (ϑ_{err}), which is defined as

$$\vartheta_{err} = \left(\frac{|M_1 - M_2|}{M_1} \times 100\right), \tag{27}$$

where M_1 and M_2 indicate the number of the actual and the detected iris pixels, respectively. M_1 is manually computed, while M_2 is computed via a row-major scanning technique [10]. Applying this method, a localized iris is considered as correct if ϑ_{err} is less 10% otherwise wrong. Accuracy comparison results are shown in Table 1. Similarly, Fig. 9(a) illustrates some randomly selected irises localized accurately using the proposed technique.

Table 1
Comparisons for the CASIA V1 iris database. (Results are taken from the published work.)

Method	Accuracy (%)
Basit [15]	99.60
Ibrahim et al. [10]	99.90
Khan et al. [7]	100.00
Wildes [8]	99.90[a]
Jan et al. [6]	100.00
Cui et al. [16]	99.34
Mateo and Rodriguez [17]	95.00[a]
Proposed	100.00

[a] Results are taken from [7].

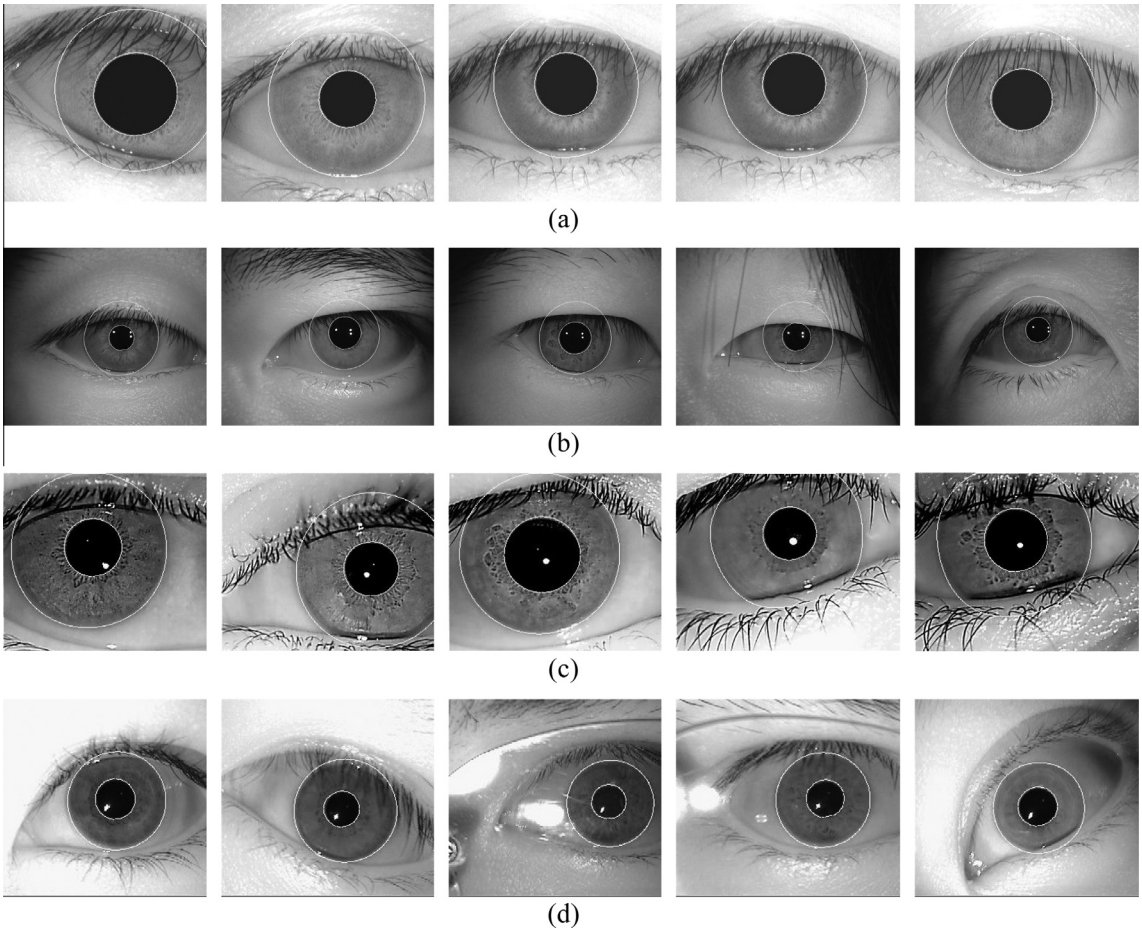

Fig. 9. (a–d) Some randomly selected accurate irises taken from the CASIA V1, CASIA-Iris-Lamp, IITD V1.0, and MMU V1.0, respectively.

3.2. Experimental Setup-II

In this setup, the CASIA-Iris-Lamp [12] was used to authenticate performance of the proposed technique. It contains 16,212 eye images collected from 411 subjects. Each image is stored in the JPEG format with resolution 640×480 pixel. Noisy factors, for instance, specular reflections, eyelashes, eyelids, hair, non-uniform illumination, etc. are common in this database. For experiment, we used a subset of only 5000 arbitrarily chosen images, and adopted the same metric, as mentioned above, to compute accuracy results (see Table 2). Fig. 9(b) illustrates some randomly selected accurately localized irises.

3.3. Experimental Setup-III

In this setup, the IITD V1.0 iris database [20] was used that includes 1120 eye images acquired from 224 subjects. Images are stored in the BMP format with resolution 320 × 240 pixel. This database contains defocus, specular reflections, rotated-irises, contact lenses, eyelashes, eyelids, and eyebrows. Table 3 shows accuracy comparison results for this database, while Fig. 9(c) illustrates some accurate iris localization results.

Table 2
Comparisons for the CASIA-Iris-Lamp iris database. (Results are taken from the published work.)

Method	Accuracy (%)
Ibrahim et al. [10]	98.28
Masek [18]	79.02[a]
Koh et al. [19]	99.00
Daugman [9]	96.00[b]
Jan et al. [6]	98.00
Proposed	99.05

[a] Results are taken from [10].
[b] Results are taken from [19].

Table 3
Comparisons for the IITD V1.0 iris database.

Method	Accuracy (%)
Jan et al. [6]	99.40
Proposed	99.46

Table 4
Comparisons results for the MMU V1.0 iris database. (Results are taken from the published work.)

Method	Accuracy (%)
Basit [15]	98.10
Masek [18]	83.92[a]
Khan et al. [7]	98.22
Jan et al. [6]	100.0
Dey and Samanta [22]	98.41[a]
Ma et al. [23]	91.02[a]
Proposed	99.55

[a] Results are taken from [7].

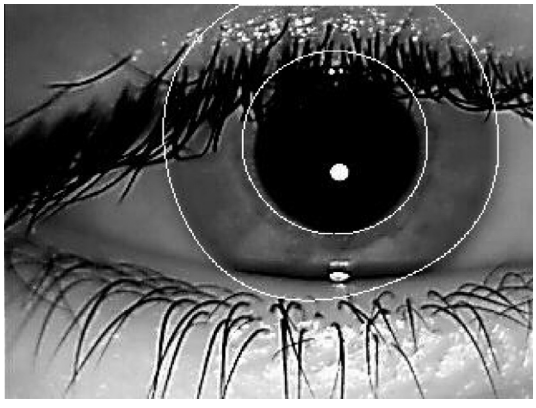

Fig. 10. Inaccurate iris localization. Here, pupil region is connected with a thick bunch of eyelashes. Image is taken from IITD V1.0.

3.4. Experimental Setup-IV

Finally, we used the MMU V1.0 [21] that includes 450 eye images collected from 45 subjects. Noisy factors, such as specular reflections, eyelashes, eyelids, and the glasses, are common herein. For experimentation, we involved all images of this database and accuracy results (see Table 4) of the proposed technique was computed using the same metric as mentioned above. Similarly, Fig. 9(d) shows some randomly selected accurate localized irises.

It is obvious from Fig. 9 that the proposed scheme is tolerant to numerous noisy factors, e.g., rotated-irises, non-uniform illumination, specular reflections; glasses, contact lenses, hair, eyelashes, and eyelids. It is experimentally observed that the proposed technique fails for an eye image (see Fig. 10) where the pupil region is severely occluded by a thick bunch of eyelashes. It is because that the gray level intensity of regions is usually close to that of the pupil.

3.5. Computational cost analysis

To compute temporal cost, we involved 2000 eye images, where 500 eye images were randomly selected from each of the used database. Furthermore, we performed computational analysis in MATALAB using its *Profile-facility*. On average, the proposed scheme took 1.5 s per eye image, which is a green indicator for the real time applications. Besides, the whole experimental setup (i.e., the MATLAB platform, WINDOWS operating system [6], and the CPU) is not real time. Therefore, the proposed technique if ported onto a dedicated media (e.g., FPGAs [6]) would surely localize an iris in less than a second.

4. Conclusion

In conclusion, this study proposed a robust iris localization technique. To localize the iris inner contour, a sliding window was first placed at a discrete location near the top-left corner of an eye image. Next, a sub image overlapped by sliding window was converted to a binary image using a multi-valued threshold. After that, a combination of the morphological opening operation and 2D object properties were adopted to localize the center and radius of a round object in that binary image. Then, parameter vector for a best round object was registered into a record, and the sliding window was shifted to a next location. This process was continued until the right-bottom corner of eye image was reached. Lastly, the iris inner contour was marked with a fine parameter vector from the record. Notably, this strategy robustly localizes the iris inner contour in the presence of noise (e.g., hair, eyebrows, eyelashes, and eyeglasses), which is an issue in most of the contemporary histogram and thresholding methods. Similarly, to localize the iris outer contour, a sub image centered at the pupil center was first extracted from eye image, where specular reflections were suppressed. Next, IDO was applied on the resultant image to localize the iris outer contour. Notably, due to the IDO, the proposed technique is tolerant to rotated-irises, which is an issue in most of the contemporary techniques. Finally, the iris contours were regularized. This scheme was tested on a set of the public iris databases. Its experimental results compared with other state-of-the-art techniques reveal its satisfactory performance.

Acknowledgments

COMSATS Institute of Information Technology, Islamabad campus Pakistan, through its in-house PhD program, supports this work. We also thank the Malaysia Multimedia University; Indian Institute of Technology Delhi; and the Chinese Academy of Sciences for providing free access to their iris databases.

References

[1] Jan F, Usman I, Agha S. A non-circular iris localization algorithm using image projection function and gray level statistics. OPTIK – Int J Light Electron Opt 2013;124:3187–93.
[2] Jan F, Usman I, Agha S. Reliable iris localization using integral projection function and 2D-shape properties. Chin Opt Lett 2012;10:111501–6.
[3] Jan F, Usman I, Khan SA. Robust iris biometric system for visible wavelength data. Chin Opt Lett 2013;11:081501–7.
[4] Jan F, Usman I, Khan SA, Malik SA. Iris localization based on the Hough transform, a radial-gradient operator, and the gray-level intensity. OPTIK – Int J Light Electron Opt 2013;124:5976–85.
[5] Bowyer KW, Hollingsworth K, Flynn PJ. Image understanding for iris biometrics: a survey. Comput Vis Image Und 2008;110:281–307.
[6] Jan F, Usman I, Agha S. Iris localization in frontal eye images for less constrained iris recognition systems. Digit Signal Process 2012;22:971–86.
[7] Khan TM, Khan MA, Malik SA, Khan SA, Bashir T, Dar AH. Automatic localization of pupil using eccentricity and iris using gradient based method. Opt Laser Eng 2011;49:177–87.
[8] Wildes RP. Iris recognition: an emerging biometric technology. Proc IEEE 1997;85:1348–63.
[9] Daugman JG. High confidence visual recognition of persons by a test of statistical independence. IEEE Trans Pattern Anal Mach Intell 1993;15:1148–61.
[10] Ibrahim MT, Khan TM, Khan SA, Khan MA, Guan L. Iris localization using local histogram and other image statistics. Opt Laser Eng 2012;50:645–54.
[11] Sankowski W, Grabowski K, Napieralska M, Zubert M, Napieralski A. Reliable algorithm for iris segmentation in eye image. Image Vis Comput 2010;28:231–7.
[12] CASIA iris database. <http://www.idealtest.org/findTotalDbByMode.do?mode=Iris> (accessed 29.04.14).
[13] Gonzalez RC, Woods RE. Digital image processing. 2nd ed. Upper Saddle River, New Jersey: Prentice Hall; 2001.
[14] Daugman J. New methods in iris recognition. IEEE Trans Syst Man Cyb Part-B 2007;37:1167–75.
[15] Basit A. Iris localization using graylevel texture analysis and recognition using bit planes Department of Computer Engineering. PhD-thesis: College of Electrical and Mechanical Engineering, National University of Sciences and Technology, Rawalpindi, Pakistan; 2009.
[16] Cui J, Wang Y, Tan T, Ma L, Sun Z. A fast and robust iris localization method based on texture segmentation. National Laboratory of Pattern Recognition, Chinese Academy of Sciences for Biometric Authentication and Testing; 2004. p. 401–8.

[17] Mateo NO, Rodriguez MAV. A fast and robust iris segmentation method. Pattern Recogn Image Anal 2007;4478:162–9.
[18] Masek L. Recognition of human iris patterns for biometric identification. BSc-Thesis: School of Computer Science and Software Engineering. The University of Western Australia; 2003.
[19] Koh J, Govindaraju V, Chaudhary V. A robust iris localization method using an active contour model and hough transform. In: Proceedings of 20th international conference on pattern recognition (ICPR). Istanbul, Turky; 2010. p. 2852–6.
[20] IITD iris database. <http://www.iitd.ac.in/> (accessed 29.04.14).
[21] MMU iris database. <http://pesona.mmu.edu.my/~ccteo/> (accessed 29.04.14).
[22] Dey S, Samanta D. A novel approach to iris localization for iris biometric processing. Int J Biol Biomed Med Sci 2008;3:180–91.
[23] Ma L, Tan T, Wang Y, Zhang D. Local intensity variation analysis for iris recognition. Pattern Recogn 2004;37:1287–98.
[24] Jan F, Usman I, Agha S. Reliable iris localization using Hough Transform, histogram-bisection, and eccentricity. Signal Process 2013;93:230–41.

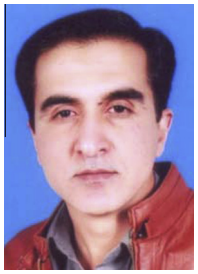

Farmanullah Jan has M.Sc. in Electronics, M.S. in Computer Engineering, and Ph.D. in Electrical Engineering. He is an Assistant Prof. at the department of Physics, CIIT, Islamabad, Pk. He is author of several journal publications, a book, and is a reviewer of some international journals. His research interests are Biometrics, Image and Digital signal processing, and Embedded systems.

Imran Usman, an Assistant Prof. at CAST, CIIT., Islamabad, Pk., received his B.S. (software engineering) degree from Foundation University, Islamabad, Pk. M.S. (Computer Systems Engineering) from Ghulam Ishaq Khan Institute of Engineering Sciences and Technology, Topi, Pk., and Ph.D. from Pakistan Institute of Engineering and Applied Sciences, Pk. His research interests include Image Processing, Watermarking, and Machine Learning.

Shahzad A. Malik is a Prof. at the Department of Electrical Engineering, CIIIT, Pk. He holds B.Sc. degree in Electrical Engineering; and the M.S. and Ph.D. degrees in the Telecommunications. His research interests include wireless and mobile networks, and integration of heterogeneous wireless networks. He is the author of several publications published in international journals.

Shahid Ahmed Khan, a Prof. at the Electrical Engineering Department, CIIT, Pk., holds B.Sc. degree in Electrical Engineering, M.Sc. in Electrical and Electronics Engineering, and Ph.D. in Communication. He has made great research contributions and has more than 40 research papers.